JOURNAL OF CATALYSIS **165,** 315–323 (1997)
ARTICLE NO. CA971509

Synthesis and Characterization of $LaCr_{1-x}Ni_xO_3$ Perovskite Oxide Catalysts

M. Stojanović,* R. G. Haverkamp,* C. A. Mims,*[,1,2] H. Moudallal,† and A. J. Jacobson†

*Department of Chemical Engineering and Applied Chemistry, University of Toronto, Toronto, Ontario M5S 3E5, Canada; and †Department of Chemistry, University of Houston, Houston, Texas 77204-5641

Received July 8, 1996; revised September 24, 1996; accepted October 30, 1996

A series of perovskite oxide catalysts with the composition $LaCr_{1-x}Ni_xO_3$ ($0 \le x \le 1$) has been synthesized by a modification of the Pechini method. The oxides have been characterized by powder X-ray diffraction, elemental analysis and surface area measurements. The $LaCr_{1-x}Ni_xO_3$ phases have the orthorhombic $GdFeO_3$ ($x < \sim 0.6$) and the rhombohedral $LaAlO_3$ structure ($x > 0.6$), in agreement with previous results. The surface and bulk compositions were shown to be equivalent by XPS measurements. Systematic changes in the binding energies of the Cr 2*p* and Ni 3*p* features are indicative of a progressive evolution of the electronic properties with nickel atom content (x). The $LaCr_{1-x}Ni_xO_3$ oxides with $x \le 0.5$ were shown by thermogravimetric analysis to be stable at 900°C in H_2/H_2O with respect to reduction to nickel metal.

INTRODUCTION

Mixed metal oxides with the perovskite structure and composition ABO_3 (A = lanthanide or alkaline earth metal and B = transition metal) find wide use as catalysts, electrocatalysts and electronic ceramics (1–3). The perovskite lattice can accommodate multiple cation substitutions with only small changes in the average structure and it is therefore an ideal model system for the study of composition–activity relations. Cation ordering and surface segregation effects can also be investigated systematically with changes in either A or B site cations. Electronic and ionic conductivity, sintering behavior, and catalytic performance are all modified by such substitutions. Specific compositions with optimized properties have been developed for application as elements in solid oxide fuel cells (SOFC) and as potential catalysts for environmental applications (4–7).

Our interest in perovskite oxides centers around their possible use as anode materials in solid oxide fuel cells (8–10). We are particularly interested in new electrode materials with mixed electron–ion conductivity that will permit direct utilization of methane at temperatures lower than currently used in SOFC technology (1000°C). Mixed electron–ion conductivity is required in order to extend the reaction zone away from the three phase contact line (gas/electrode/electrolyte) over the entire electrode surface. In addition to high electronic and ionic conductivity, a material suitable for use as fuel side electrode must satisfy several other criteria. The surface must effectively catalyze the half-cell reaction to reduce polarization effects arising from surface kinetics and the material must be thermodynamically stable under normal and upset conditions ($pO_2 \sim 10^{-19}$ atm). Interphase contact and adhesion, compatibility with the oxide electrolyte with respect to reaction, and thermal expansion and ease of fabrication, are also significant concerns. Developing an oxide material that will satisfy these criteria simultaneously is a significant challenge. Design of new perovskite oxides, taking advantage of the compositional flexibility, offers the best current prospect for improved materials and is an active research area.

Only $LaCrO_3$ of the perovskite series $LaMO_3$ (M = Cr, Mn, Fe, Co, Ni) has the stability required for use as a fuel side electrode (9). $LaCrO_3$-based oxides are consequently the focus of the present work. The pure oxide has low catalytic activity though some data have been reported for methane combustion and coupling chemistry (6, 7, 11). Other members of the series $LaMO_3$ (M = Cr, Mn, Fe, Co, Ni, Ru) and doped $La_xSr_{1-x}MO_3$ are active catalysts for methane combustion with TOF > 10/s at 600°C (6, 7). The relative activities of these catalysts have a positive correlation with their ease of reduction and are more active than $LaCrO_3$. In principle, the oxidation activity of $LaCrO_3$ can be improved by substitution of either the A or B site cations. Previous catalytic studies have concentrated on the effects of A site substitution, for example, in $La_{0.8}Ca_{0.2}CrO_3$ (12). This compound has also been considered as a potential anode material (13). Substitution of $LaCrO_3$ on the B sites with more reducible transition metals, for example Co^{3+} and Ni^{3+} is also expected to increase catalytic activity. Some data suggest that these transition metal

[1] To whom correspondence should be addressed.
[2] Fax: (416) 978-8605. E-mail: Mims@ecf.toronto.edu.

0021-9517/97 $25.00

cations are stabilized with respect to reduction and phase separation in $LaCr_{1-x}M_xO_3$ compositions (14–16). Additional information on the structural chemistry and properties of $LaCr_{1-x}M_xO_3$; $M = Co, Ni$ has been reported recently (16–21).

In this paper, we report a study of the effects of Ni substitution for Cr on the bulk structure, stability with respect to reduction under low pO_2 conditions, and surface composition of $LaCr_{1-x}Ni_xO_3$ with $0 \leq x \leq 1$. In part II, the details of the methane combustion kinetics are described as a function of catalyst composition. A neutron diffraction study of the structures of specific oxidized and reduced phases and other properties of these materials relevant to SOFC applications will be described in succeeding papers in this series.

EXPERIMENTAL METHODS

Sample Preparation

The $LaCr_{1-x}Ni_xO_3$ ($x = 0$, 0.1, 0.2, 0.25, 0.3, 0.4, 0.5, 0.6, 0.7, 0.75, 1.0) samples were synthesized using a modification of the Pechini method (series A) (22). Duplicate syntheses ($x = 0$, 0.25, 0.5, 0.75, 1.0) generated materials for the detailed kinetics studies (series B). The starting materials used were ethylene glycol (99+%), citric acid (99.5+%), chromium (III) nitrate nonahydrate (99.99+%), lanthanum oxide (99.999%), and nickel (II) nitrate hexahydrate from Aldrich. Lanthanum oxide was heated at 800°C before use to remove adsorbed water and carbon dioxide. The chromium and nickel contents of the hydrated chromium and nickel nitrates were determined by gravimetric analysis as barium chromate and by thermal decomposition to nickel oxide, respectively. Solutions were prepared with the appropriate stoichiometries by dissolving the nitrates and lanthanum oxide in enough dilute nitric acid to yield $[La] = 0.01$ *M*. These nitrate solutions were combined with an ethylene glycol/citric acid gel which was prepared separately. Citric acid (4 g) was dissolved in 2 mL hot water to which was added 0.9 mL ethylene glycol and a drop of concentrated nitric acid. This mixture was covered and stirred on a hot plate until it formed a viscous gel. The nitrate solution was then added to the gel and the mixture heated at 60°C until homogeneous. The solution (about 100 mL in total volume) was then transferred to a 1-L beaker and placed in a drying oven at 120°C for 1 h. The temperature was then slowly raised to 250°C over a period of 1–2 h. The removal of water and subsequent heating causes the solution to foam and eventually fill the beaker with a dry foamed resin. This resin was ground and calcined at 760°C for ~4 h (series A) or 2 h (series B) to produce the final materials.

Deviations from perfect stoichiometry in the binary and ternary materials necessarily result in small quantities of other phases, which if active and highly dispersed, can skew the catalytic results (6). Reference samples (series C) were also prepared and characterized by XPS in order to examine this issue. Samples of the single component oxides (NiO and La_2O_3 (both 99.99% pure) and Cr_2O_3 (99.995%)) were obtained from Aldrich. La_2NiO_{4+x} was prepared by a standard ceramic technique. Stoichiometric amounts of La_2O_3 (predried at 800°C, Aldrich 99.9%) and NiO (Aldrich 99.99%) were ground and heated at 1250°C. The sample was then pelletized and heated to 1380°C for 12 h. Nickel oxide was purposely added to $LaCr_{0.25}Ni_{0.75}O_3$ by solution addition (incipient wetness) with sufficient nickel nitrate to produce 5 wt% nickel oxide. Another mixed-phase material was produced by destructive reduction of $LaCr_{0.25}Ni_{0.75}O_3$ in wet (saturated by water vapor at 25°C) hydrogen at 450°C. A modification of the synthetic method was also used to minimize the production of other phases. Excess lanthanum (usually 50%) was included in the original solution, which assures complete incorporation of the "B" cations into mixed metal oxides during gelation and calcination (23). All compounds formed from the excess lanthanum oxide can be leached selectively from the resulting material in citric acid. The formation of La_2NiO_4 prevents the use of this method to synthesize $LaNiO_3$ but for other ternary oxides satisfactory results can be obtained. A sample with nominal $LaCr_{0.5}Ni_{0.5}O_3$ stoichiometry was produced in this way for the kinetic studies.

Sample Characterization

The sample compositions were determined by Inductively Coupled Plasma Emission Spectroscopy (ICPES) using a Perkin-Elmer ICP/5500 instrument. Standard solutions of the individual metals (each at 10, 50, and 100 ppm concentrations) were prepared by dissolving La_2O_3 (preheated at 800°C), NiO and $K_2Cr_2O_7$ in dilute nitric acid. The $LaCr_{1-x}Ni_xO_3$ samples were dissolved in dilute nitric acid and diluted to give concentrations in the 10–100 ppm range. Single standards were used for calibration and there were no interferences. The analysis of each sample was performed in triplicate. The phase purity of the solids was characterized by X-ray powder diffraction using a Scintag XDS2000 automated diffractometer. (Cu$K\alpha$ radiation, $\lambda = 1.54178$ Å, flat plate sample, θ–θ geometry). Step scan data were collected in 0.02° steps with a count time of 6 s per step over the angular range $15° < 2\theta < 120°$. All samples were single phase with either an orthorhombic or rhombohedrally distorted perovskite structure. The diffraction patterns were fitted by Rietveld refinement using the program GSAS (24) locally modified to run on a microVAX 3100 computer. Precise values for the lattice constants were thus obtained, but since the data are relatively insensitive to the oxygen atom positions, no attempt was made to extract detailed structural information.

TABLE 1

Surface and Bulk Compositions of $LaCr_{1-x}Ni_xO_3$ Perovskite Oxides

Series	Composition	Bulk (Cr + Ni)/La	Bulk Ni/(Ni + Cr)	Surface (Cr + Ni)/La	Surface Ni/(Ni + Cr)	Surface area ($m^2\ g^{-1}$)
A	$LaCrO_3$	0.99	0	0.97	0	3.3
A	$LaCr_{0.9}Ni_{0.1}O_3$	1.05	0.095	—	—	4.4
A	$LaCr_{0.8}Ni_{0.2}O_3$	1.03	0.194	—	—	3.5
A	$LaCr_{0.75}Ni_{0.25}O_3$	1.02	0.245	1.14	0.28	2.5
A	$LaCr_{0.7}Ni_{0.3}O_3$	1.04	0.29	—	—	3.4
A	$LaCr_{0.6}Ni_{0.4}O_3$	1.01	0.40	—	—	3.1
A	$LaCr_{0.5}Ni_{0.5}O_3$	1.01	0.49	1.07	0.44	3.5
A	$LaCr_{0.4}Ni_{0.6}O_3$	0.98	0.59	1.13	0.60	5.2
A	$LaCr_{0.3}Ni_{0.7}O_3$	—	0.68	—	—	4.4
A	$LaCr_{0.25}Ni_{0.75}O_3$	1.00	0.74	1.20	0.70	2.9
A	$LaNiO_3$	1.00	1	1.05	1.0	3.3
B	$LaCrO_3$	—	—	0.95	0	4.9
B	$LaCr_{0.75}Ni_{0.25}O_3$	—	—	0.80	0.19	6.6
B	$LaCr_{0.5}Ni_{0.5}O_3$	—	—	0.67	0.47	8.6
B	$LaCr_{0.25}Ni_{0.75}O_3$	—	—	0.71	0.71	7.9
B	$LaNiO_3$	—	—	0.83	1.0	8.1
C	$LaCr_{0.5}Ni_{0.5}O_3$	—	—	0.74	0.32	6.1
C	$NiO + B(Ni_{0.75})$	—	—	—	0.76	4.2

The surface areas of the materials were measured on an Omnisorb 100CX analyzer using nitrogen adsorption at 77 K and the BET method. Prior to the adsorption measurements, the samples were outgassed at 300°C for 3 h. The surface areas of the Series A samples were systematically lower than those of series B (see Table 1) most probably because the series A samples were held at the final calcination temperature for a longer time (~4 h rather than 2 h).

The relative stabilities of the $LaCr_{1-x}Ni_xO_3$ oxides in reducing atmospheres were determined by thermogravimetric reduction in a 5% H_2/95% N_2 stream that was presaturated with water vapor at ambient temperature. The measurements were made using a DuPont-951 thermogravimetric analyzer. The temperature was raised at 10°C/min to 120° and held for 15 min to remove any adsorbed water and then raised at 5°C/min to 900°C and held for 2 h.

Surface compositions were measured on an LH-11 XPS analyzer (A series, 100 eV pass energy, Mg$K\alpha$, $\gamma = 90°$) and a Leybold MAX 200 XPS analyzer (B series, 48 eV pass energy, Al$K\alpha$, $\gamma = 54.4°$) both equipped with unmonochromatised X-ray sources. The samples were imbedded in graphite disks 11 mm in diameter and introduced into the system through an atmospheric pressure load-lock. The background pressure was less than 10^{-8} Torr. Only cation distributions were calculated since adventitious carbon and oxygen on the surface precluded quantitative oxygen analysis. The accumulated spectra were adjusted to place the prominent C 1*s* peak at 285.0 eV. Peak intensities were obtained by curve fitting using instrument supplied software that included X-ray satellite line subtraction based upon a program by van Attekum and Trooster (25) and published background subtraction procedures (26). All peak areas were corrected for published ionization cross-sections (27), attenuation path lengths (28), angular asymmetry factors (29), and spectrometer terms.

RESULTS AND DISCUSSION

Table 1 lists the pervoskite compounds synthesized, their measured bulk and surface compositions, and their surface areas.

X-Ray Diffraction Results

$LaCrO_3$ has the orthorhombic $GdFeO_3$ structure at room temperature, space group *Pnma* (#62), $Z = 4$ (30). The lattice parameters and esds as determined using GSAS were $a = 5.4771(4)$Å, $b = 7.7620(5)$Å, $c = 5.5197(4)$Å; the numbers in parentheses refer to the uncertainty in the last digit. $LaNiO_3$ is rhombohedral at room temperature, space group $R\bar{3}c$ (#167), $Z = 2$ (31). The lattice parameters were $a = 5.4033(8)$Å and $\alpha = 60.620(5)°$. The intermediate $LaCr_{1-x}Ni_xO_3$ compositions have either the orthorhombic $LaCrO_3$ structure for $x \leq \sim 0.6$ or the rhombohedral $LaNiO_3$ structure ($x \geq 0.7$). The variation of the lattice parameters with composition is shown in Fig. 1 and the values are listed in Table 2. To facilitate comparisons, the orthorhombic cell parameters were transformed into pseudocubic cell parameters (a_c) using the relations $a = b = a_c\sqrt{2}$, $c = 2a_c$, and a mean "cubic" cell parameter calculated as $\langle a \rangle = V^{1/3}$. For the samples with rhombohedral structures, the cell volume was obtained from the

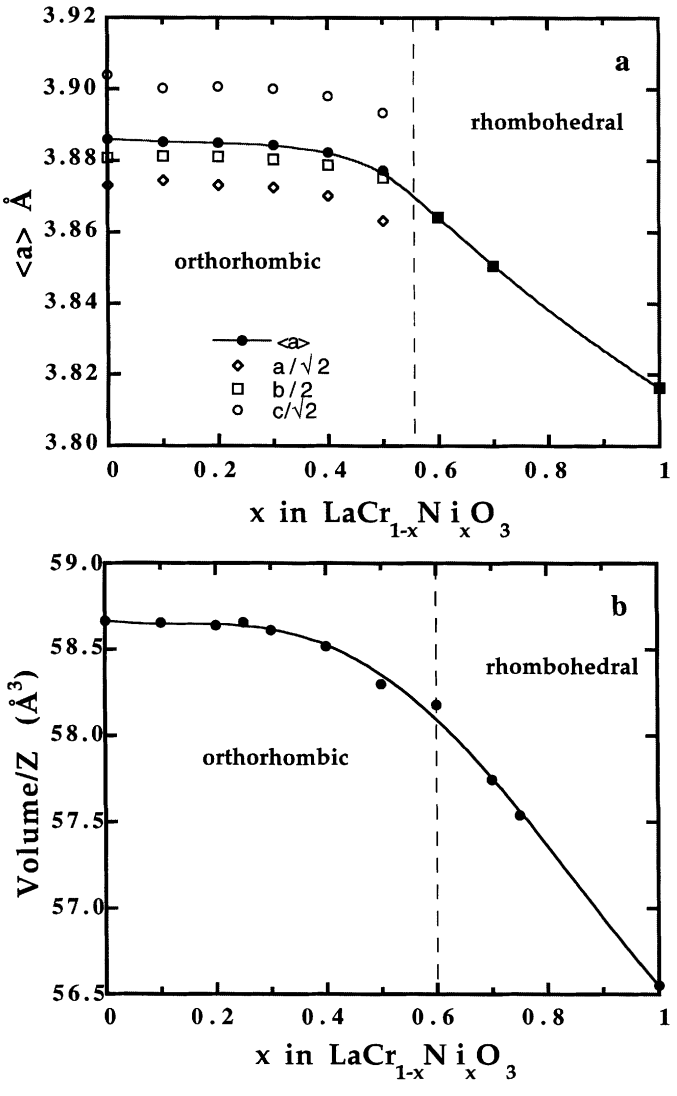

FIG. 1. (a) Lattice parameters of $LaCr_{1-x}Ni_xO_3$ oxides as a function of x; (b) unit cell volumes.

parameters (a_r, α) and used to calculate the pseudocubic cell constant, $a_c = V_r^{1/3}$. The variation of cell volumes with composition, normalized to account for the difference in Z, is shown in Fig. 1b. The average pseudocubic cell constant and the cell volume show a smooth variation with composition as expected for a continuous solid solution. The results are in good agreement with the data reported by Höfer *et al.* (20). It should be noted that the average pseudocubic cell constants reported in Ref. (20) are estimated differently. The present samples show significant line broadening consistent with the method of preparation and the measured surface areas. Consequently, it is difficult to distinguish between the orthorhombic and rhombohedral phases as the transition is approached in composition. The present data indicate that the structure change occurs at $x \sim 0.6$ which is in the range reported previously ($x = 0.5$–0.65) (15, 20, 21). We note that the transition between the orthorhombic *Pnma* and rhombohedral $R\bar{3}c$ structures is expected to be first order and that therefore a two-phase region should exist between the two structure types. The line widths and the composition resolution in the present series of samples preclude the observation of this two phase region but it has been observed in the corresponding $LaCr_{1-x}Co_xO_3$ system (17). No impurity phases were detected in the X-ray diffraction patterns. By comparison with simulated diffraction patterns of mixtures, an upper limit of 2 wt% NiO impurity in $LaNiO_3$ is indicated. The reference materials La_2NiO_4, La_2O_3, Cr_2O_3, NiO were all single phase by X-ray diffraction.

Reduction Stability

The thermogravimetric reduction data, following the initial dehydration, are shown in Fig. 2 and the results tabulated in Table 3. As expected from thermodynamics under the conditions used (the equivalent pO_2 at 1000°C of 5% H_2 saturated with water at ambient temperature is 10^{-17} atm), $LaCrO_3$ does not reduce. The nickel-containing samples, however, all show one or more distinct reduction stages. $LaNiO_3$ reduces in two steps; the first between 180 and 400°C corresponds to the reduction of Ni^{3+} to Ni^{2+} and the formation of $LaNiO_{2.5}$ (32, 33). The second reduction step between 450 and 550°C corresponds to complete reduction to Ni metal and La_2O_3, confirmed by X-ray diffraction of the residue.

All of the ternary perovskites also show a weight loss below 400°C corresponding to reduction of Ni^{3+} to Ni^{2+}. For $x > 0.5$, this reduction to Ni^{2+} is complete. Further reduction of these materials to Ni metal occurs as the temperature is increased. The reduction occurs continuously over a range of temperature (Fig. 2, $x = 0.7$) suggesting a mechanism in which Ni metal is formed together with a more chromium-

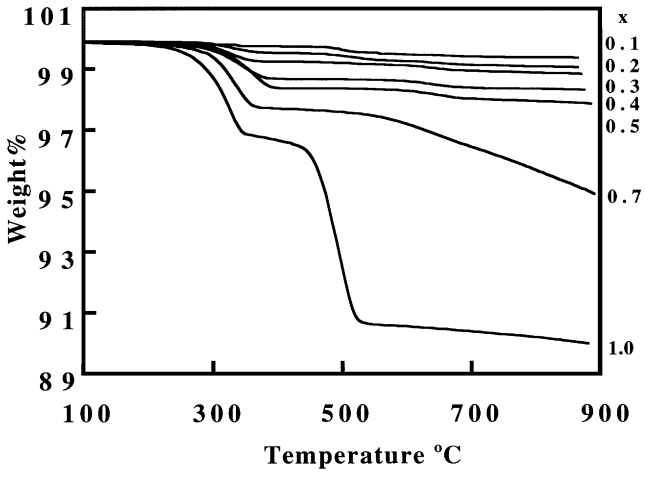

FIG. 2. Thermogravimetric reduction of $LaCr_{1-x}Ni_xO_3$ at 5°C/min in 5% H_2 saturated with water vapor at ambient temperature.

TABLE 2

Lattice Parameters for $LaCr_{1-x}Ni_xO_3$ Perovskite Oxides

Composition	a(Å)	b(Å)	c(Å)	α(°)	V(Å^3)	V(Å^3)/Z
$LaCrO_3$	5.4771(4)	7.7620(5)	5.5197(4)	—	234.66	58.66
$LaCr_{0.9}Ni_{0.1}O_3$	5.4795(2)	7.7628(4)	5.5160(2)	—	234.63	58.66
$LaCr_{0.8}Ni_{0.2}O_3$	5.4775(3)	7.7625(4)	5.5166(3)	—	234.56	58.64
$LaCr_{0.75}Ni_{0.25}O_3$	5.4770(6)	7.7663(9)	5.5165(6)	—	234.65	58.66
$LaCr_{0.7}Ni_{0.3}O_3$	5.4767(2)	7.7610(3)	5.5158(2)	—	234.45	58.61
$LaCr_{0.6}Ni_{0.4}O_3$	5.4734(4)	7.7578(4)	5.5127(2)	—	234.08	58.52
$LaCr_{0.5}Ni_{0.5}O_3$	5.4608(6)	7.7554(9)	5.5062(6)	—	233.19	58.30
$LaCr_{0.4}Ni_{0.6}O_3$	5.4650(4)	—	—	60.363(4)	116.36	58.18
$LaCr_{0.3}Ni_{0.7}O_3$	5.4457(3)	—	—	60.504(3)	115.50	57.75
$LaCr_{0.25}Ni_{0.75}O_3$	5.4328(4)	—	—	60.666(2)	115.09	57.54
$LaNiO_3$	5.4033(8)	—	—	60.620(5)	113.11	56.55

rich perovskite phase according to the reaction

$$(1-y)LaCr_{1-x}Ni_xO_3 \rightarrow (1-x)LaCr_{1-y}Ni_yO_{3-y/2} + (x-y)Ni + ((x-y)/2)La_2O_3.$$

The extent of this process depends strongly on composition and is governed by the stability of the residual ternary perovskite phases as well as by cation mobilities. For materials with $0 < x \leq 0.5$ the reduction to Ni^{2+} is not complete in the first wave at 400°C. We assign this feature to the reduction of Ni^{3+}–O–Ni^{3+} ensembles and the amounts are consistent with a statistical distribution of Ni on the B sites in the lattice. The remaining Ni^{3+} does reduce to Ni^{2+} by 800°C in two subsequent poorly resolved processes. The $LaCr_{1-x}Ni_xO_3$ compounds with $x < 0.5$ do not reduce to nickel metal under these conditions at ≤900°C. A more detailed analysis of the reduction of these materials will be published elsewhere (34).

TABLE 3

Thermogravimetric Weight Loss (100–420°C) in $LaCr_{1-x}Ni_xO_3$[a]

x in $LaCr_{1-x}Ni_xO_3$	Formula weight, g	δ in $LaCr_{1-x}Ni_xO_{3-\delta}$	
		Theoretical[b]	Measured[c]
0.0	238.90	0.00	0.0
0.1	239.57	0.05	0.02
0.2	240.24	0.10	0.05
0.25	240.58	0.125	0.09
0.3	240.91	0.15	0.10
0.4	241.58	0.20	0.16
0.5	242.25	0.25	0.22
0.6	242.92	0.30	0.27
0.7	243.59	0.35	0.33
0.75	243.92	0.375	0.34
1.0	245.60	0.5	0.48

[a] Data from Fig. 5, weight loss during the first reduction wave ($T < 420$°C) in 5%H_2/95%N_2 saturated with water at ambient temperature ($pH_2O = 5$ kPa), total pressure = 100 kPa.

[b] Amount associated with complete reduction of Ni^{3+} to Ni^{2+}.

[c] The estimated errors in the measured composition are ±0.005.

XPS Characterization and Surface Compositions

Various spectral regions of $LaCr_{1-x}Ni_xO_3$ ($x = 0.0$, 0.25, 0.5, 0.75, 1.00) are shown in Figs. 3–5. The features used in the analysis were La $3d_{5/2}$, split into two final-state components at nominal binding energies 835 eV (La_I) and 838 eV (La_{II}), La 4*d* (103–106 eV), Cr $2p_{3/2}$ (574 eV) and 3*p* (43 eV), Ni 3*p* (67 eV) and $2p_{1/2}$ (870 eV), and O 1*s*, comprised of an oxide component (530 eV) and higher binding energy components centered around 533 eV. The surface cation

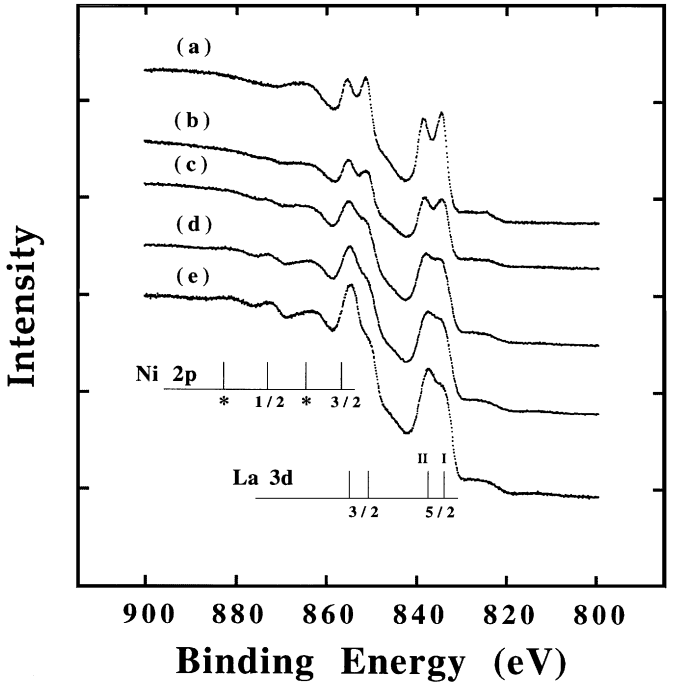

FIG. 3. XPS spectra (Ni 2*p*, La 3*d* region) of $LaCr_{1-x}Ni_xO_3$ oxides, (a) $x = 0$, (b) $x = 0.25$, (c) $x = 0.5$, (d) $x = 0.75$, (e) $x = 1.00$ (*denotes shakeup).

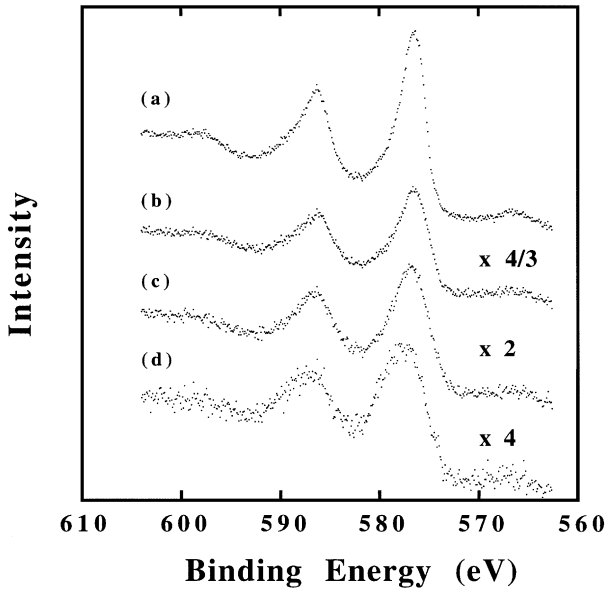

FIG. 4. XPS spectra (Cr 2*p* region) of $LaCr_{1-x}Ni_xO_3$ oxides, (a) $x = 0$, (b) $x = 0.25$, (c) $x = 0.5$, (d) $x = 0.75$. The intensity data in the *b*, *c*, and *d* spectra are normalized to the $x = 0$ spectrum by the factors shown.

compositions of all the materials were derived from La $3d_{5/2}$, Cr 2*p* and Ni 3*p* features (calibrated by Ni 2*p* — see below). These Ni/La and Cr/La ratios are plotted in Fig. 6 and listed in Table 1. Some details of the analysis are worth mentioning. The prominent nickel 2*p* feature overlaps with the complex La 3*d* region (see Fig. 3), and shows the extensive shakeup features characteristic of oxidized forms. Attempts to extract reliable Ni $2p_{3/2}$ intensity from this region were not successful, leaving the much less intense and somewhat asymmetric 3*p* peak as the only nickel feature available for all the samples. Even so, the close proximity of Cr 3*s* (75 eV B.E.) interferes with accurate determination of the background in the data for the ternary perovskites. Accordingly, a limited portion (from 7 eV below the high kinetic energy edge) of the Ni 3*p* peak was analyzed for all materials, thus excluding a portion (35% on $LaNiO_3$) of the area. Reliable Ni $2p_{1/2}$ areas were obtainable from the nickel rich materials ($x = 0.5$, 0.75, and 1.0) and these were used to calibrate the Ni 3*p* intensities. Figure 6 shows that the derived surface Cr/La ratios and Ni/La ratios are similar to the bulk values, for all the perovskites, including La_2NiO_4.

The forgoing analysis assumes homogeneous materials, but distinct surface compositions are possible and of obvious interest. The XPS intensities from there granular samples contain contributions from several atomic layers and from a distribution of takeoff angles. Layer by layer simulations of the XPS spectra were used to examine the uncertainties in surface composition associated with the finite

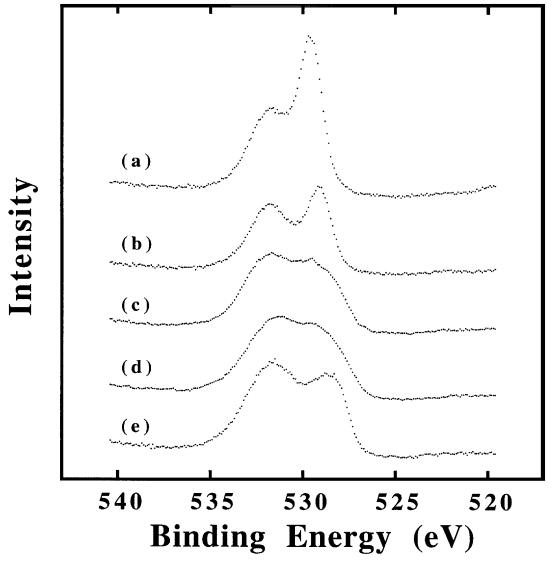

FIG. 5. XPS spectra (O1*s* region) of $LaCr_{1-x}Ni_xO_3$ oxides, (a) $x = 0$, (b) $x = 0.25$, (c) $x = 0.5$, (d) $x = 0.75$, (e) $x = 1.00$.

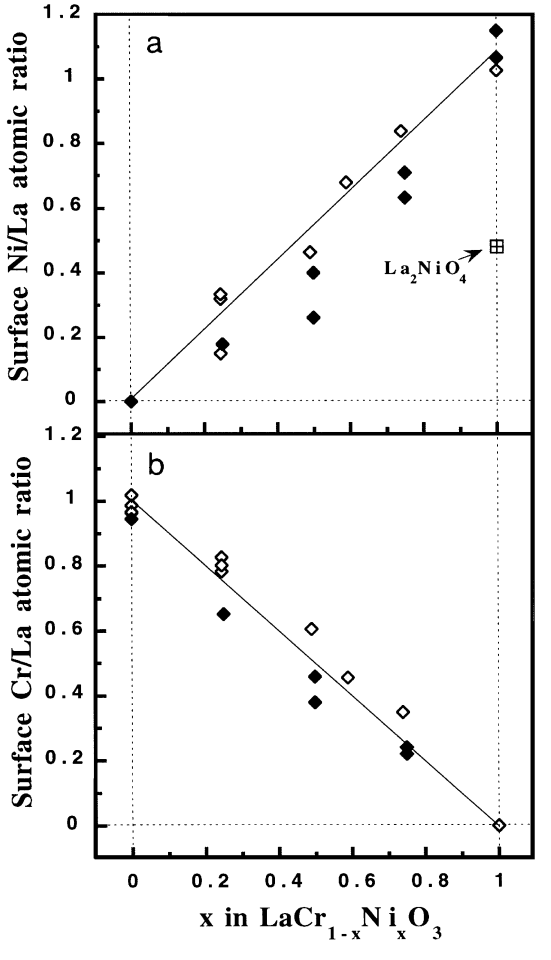

FIG. 6. Variations of surface Ni/La (panel a) and Cr/La (panel b) ratios with *x* in $LaCr_{1-x}Ni_xO_3$. Open symbols refer to series A and closed symbols to series B.

sampling depth of XPS. Two types of distributions with distinct Cr/Ni compositions in the top layer were investigated: one with homogeneous A/B ratios and the other with alternative A or B cation containing layers. For a flat sample, a wide latitude of top layer compositions is consistent with the data. For example, a sample with bulk composition $LaCr_{0.5}Ni_{0.5}O_3$ with the top atomic layer composition $LaCrO_3$ would yield a Cr/La XPS ratio (30° takeoff angle) of 0.59, in the range of measured values. The importance of high takeoff angles on powder samples, however, decreases the average sampling depth and makes the measurements more surface sensitive (35, 36). Although difficult to quantify for our samples, simulations of photoemission from hemispheres of the same material considered in the flat sample calculation above would yield a Cr/La ration of 0.65. The calculated Cr/La ratios for hemispherical $LaCrO_3$ are 0.65 and 1.5 for samples terminated by A-only and B-only layers, respectively. While these calculations show the possible variation for an individual sample, a distinct B composition in the top layer would yield a nonlinear relationship between the surface and bulk compositions over the entire series—a trend not seen in the data. Cr/La ratios derived from the Cr 3*p* and La 4*d* features (higher kinetic energy) were similar to those from Cr 2*p* and La 3*d*. The different attenuation lengths provide modest depth profiling information and the similar Cr/La ratios and the proportionality to bulk values in both cases argues against any strong concentration gradients. In summary, the surface compositions of these materials are indistinguishable from the bulk values.

Figure 7 illustrates the systematic variations in the spectra with composition. The XPS binding energies, particularly of Ni and Cr, shift with increasing Ni substitution. The binding energies of Ni 3*p*, Cr 2*p* and O 1*s* (oxide) are plotted relative to La 3*d*, which is, in turn, relatively constant with respect to the adventitious carbon peak. The nickel binding energies in $LaNiO_3$ are approximately 1 eV higher than in La_2NiO_4, consistent with the higher nominal charge state. In the presence of Cr in the lattice, however, the Ni 3*p* binding energies are lowered until, for dilute Ni systems, they approach those of La_2NiO_4. The concomitant increase in Cr 2*p* binding energies as Ni is introduced into the lattice indicates a sharing of electron density between Ni and the less electronegative Cr. The shift in Cr 2*p* binding energy with *x* involves the wholesale movement of the peak with little change in shape except for a small amount of broadening (Fig. 4). In addition to the small shift in the oxide component of the O 1*s* with increasing nickel content, the relative intensity of the higher binding energy component increases systematically with increasing nickel content (see Fig. 5). Similar effects have been seen in other investigations and attributed variously to O^-, surface oxygen/adsorbed O_2, hydroxyl groups, and adventitious material (2). These assignments remain unclear since most samples, like ours, have been exposed to atmosphere prior to analysis.

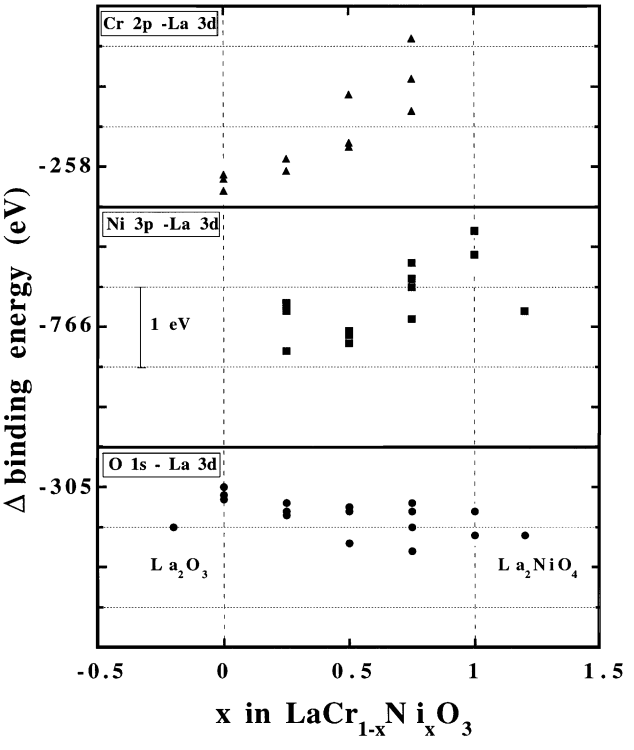

FIG. 7. Variations in binding energies with *x* in $LaCr_{1-x}Ni_xO_3$.

The relative intensity of the higher binding energy component of La $3d_{5/2}$ (La_{II}) increases systematically with composition. This trend, apparent in Fig. 3, is plotted in Fig. 8. This well-known and extensively investigated (37–44) phenomenon is generally agreed to result from mixed final states derived from hybridization of valence levels with La

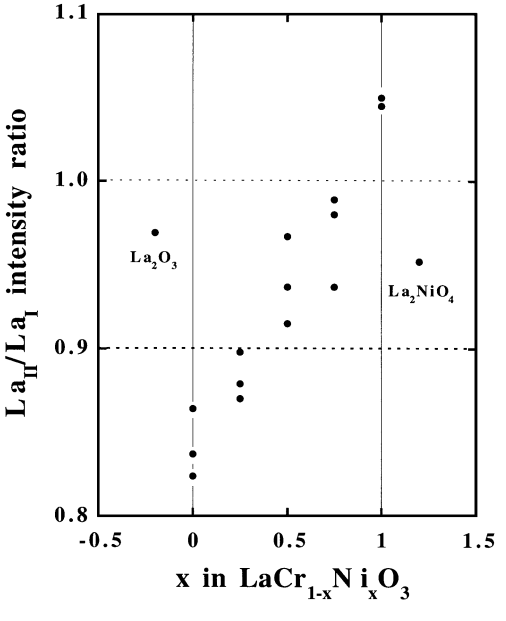

FIG. 8. Variation in the La_{II}/La_I XPS intensity ratio.

4*f* levels (40, 42, 44) in the presence of the 3*d* core hole. The details of the intensity variations are therefore complex but the relative intensity of La_{II} correlates with the covalent tendencies of the counter ions (ligands) (37). The Ni 3*d*-O 2*p* levels are strongly mixed in $LaNiO_3$ to form itinerant states of the conduction band (39, 45) and it is therefore consistent that increased mixing with nearby La 4*f* levels should also result. Along with the change in peak intensity ratios the separation between the main peak and the satellite decreases slightly from $LaCrO_3$ (3.8 eV) to $LaNiO_3$ (3.5 eV) again consistent with previous trends (37).

Similarities and differences are noted between these results and previous studies of related systems. Previous measurements (46) of the surface composition of $LaNiO_3$ (Ni/La = 0.41) and La_2NiO_4 (Ni/La = 0.23) differ from ours, although no details of these analyses were provided. Similar to our findings, the surface Cr/La and Co/La ratios of the substitutional series $LaCr_{1-x}Co_xO_3$ were reported to be proportional to bulk values (18) although the B/La ratios were lower than in the bulk and there was some evidence of surface chromium enrichment. The shift of the Cr 2*p* levels here contrasts with the case of substitution of Ba(Sr) on A sites in $LaCrO_3$ (38). In this study, discrete Cr^{4+} sites, necessary to achieve local charge balance around the substitutions, were clearly seen in XPS. The appearance of a similar high valent Cr feature also accompanies Co substitution in $LaCr_{1-x}Co_xO_3$ (18). The changes in $LaCr_{1-x}Ni_xO_3$, on the other hand, result from nonlocal responses in the valence levels, consistent with the substantial conductivity of these materials (20). The effect of nickel substitution decreases the O 1*s* oxide binding energy only slightly, if at all, and has no consistent effect on La 3*d* peak positions—most of the movement involves the B site ions. By contrast, in the $LaCr_{1-x}Co_xO_3$ series, slight (magnitudes not stated) shifts to higher binding energies were reported for La, Co, and O, but not for the Cr peaks (18). The increased electronegativity difference between Ni and Cr and the formation of metallic conduction is responsible for the more pronounced effects here. The La 3*d* splitting is consistent with other results in perovskites. The intensity of the La_{II} component increases in the series $LaMO_3$ (M = Ti–Co) (39), with A site substitutions (38, 47) and with Co substitution in $LaCr_{1-x}Co_xO_3$ (18). The high binding energy oxygen observed here is consistent with the systematics of previous investigations. Its intensity in as-prepared samples increases in the series $LaMO_3$ (M = Ti–Co) (39, 48) and with Co substitution in $LaCr_{1-x}Co_xO_3$ (18). This feature has been related, not without controversy, to the ease of reduction and increased catalytic activity (46, 48, 49). This oxygen feature also correlates with increased catalytic activity of $LaCr_{1-x}Ni_xO_3$ (50), in agreement with previous trends, but the details are far from clear.

No changes were detected in the surface compositions after exposure to high temperatures (500°C) in vacuum or after extensive use as a methane oxidation catalyst at temperatures up to 600°C providing the reaction did not proceed to oxygen starvation. Destructively reduced samples which were subsequently oxidized in oxygen containing atmospheres showed Ni XPS consistent with the formation of Ni^{2+} materials such a La_2NiO_4 and NiO.

SUMMARY AND CONCLUSIONS

A series of catalysts with compositions $LaCr_{1-x}Ni_xO_3$, $0 \le x \le 1.0$ has been synthesized by a modification of the Pechini method. The samples are single phase with moderate surface areas in the range 2–9 m^2/g. Powder X-ray diffraction measurements show that chromium-rich compositions have the orthorhombic $GdFeO_3$ structure up to $x = \sim 0.6$. $LaNiO_3$ and composition with $x > 0.6$ have the rhombohedral $LaAlO_3$ structure (51). The lattice parameters and unit cell volumes of the $LaCr_{1-x}Ni_xO_3$ series show a strong positive deviation from Vegard's law. At low nickel concentrations, the lattice constant is apparently determined by the Cr–O–Cr distance and remains almost constant until the nickel concentration reaches a value corresponding to $x = 0.4$. For $x > 0.4$, the pseudocubic cell constant decreases smoothly to the value of $LaNiO_3$. The behavior is in marked contrast to that of the $LaCr_{1-x}Co_xO_3$ system which shows a negative deviation from Vegard's law and a transition from the orthorhombic $LaCrO_3$ structure to the rhombohedral phase at a lower level of substitution ($x = \sim 0.2$) (17).

Analysis of the XPS spectra indicates that the surface compositions of the $LaCr_{1-x}Ni_xO_3$ phases are indistinguishable from the bulk values. Similar results were reported for $LaCr_{1-x}Co_xO_3$ (18). The XPS data for the nickel substituted phases show very little evidence for the presence of chromium species other than Cr^{3+} but do show systematic shifts with x in the Ni 3*p* and Cr 2*p* features to higher and lower binding energies, respectively. The XPS data for the cobalt compounds show several differences from the corresponding nickel series. In particular, a pronounced feature at higher binding energy in the Cr $2p_{3/2}$ region was interpreted as indicating the presence of a significant amount of Cr^{4+}. Also in contrast to the nickel system, the chromium peaks remain at the same position for all compositions but the Co features shift to lower binding energies with increasing x. The XPS, structural data and the much higher conductivities ($\times 10^3$) observed for $LaCr_{1-x}Ni_xO_3$ (18) compared to $LaCr_{1-x}Co_xO_3$ (16) all indicate that the two systems have a markedly different charge distribution on the B sites.

$LaCr_{1-x}Ni_xO_3$ compositions with $x \le 0.5$ were shown by thermogravimetric analysis in H_2/H_2O to be stable with respect to reduction to nickel metal at temperatures below 900°C. These compositions are therefore sufficiently stable to be used as anode materials in solid oxide fuel cells. Catalytic properties of the $LaCr_{1-x}Ni_xO_3$ materials for

methane oxidation, relevant to this application are described in an accompanying paper (50).

ACKNOWLEDGMENTS

The authors thank Mark Bellino and Nathan Joos for some sample preparations and E. Stern for helpful discussions. Support by a Collaborative Project Grant from the Natural Science and Engineering Research Council of Canada (CAM) and from The Texas Center for Superconductivity and the Robert A. Welch Foundation (AJJ) is gratefully acknowledged.

REFERENCES

1. Tejuca, L. J., Fierro, J. L. J., and Tascon, J. M. D., *Adv. Catal.* **36**, 237 (1989).
2. Tejuca, L. J. and Fierro, J. L. J., "Properties and Applications of Perovskite-Type Oxides," Dekker, New York, 1993.
3. Voorhoeve, R. J. H., Johnson, D. W., Jr., Remeika, J. P., and Gallagher, P. K., *Science* **195**, 827 (1977).
4. Minh, N. Q., *J. Am. Ceram. Soc.* **76**, 563 (1993).
5. Minh, N. Q., and Takahashi, T., "Science and Technology of Ceramic Fuel Cells," Elsevier, Amsterdam, 1995.
6. McCarty, J. G., and Wise, H., *Catal. Today* **8**, 231 (1990).
7. Arai, H., Yamada, T., Eguchi, K., and Seiyama, T., *Appl. Cat.* **26**, 265 (1986).
8. Steele, B. C. H., Kelly, I., Middleton, H., and Rudkin, R., *Solid State Ionics* **28–30**, 1547 (1988).
9. Steele, B. C. H., Middleton, P. H., and Rudkin, R. A., *Solid State Ionics* **40/41**, 388 (1990).
10. Mogensen, M., and Bentzen, J. J., *in* "Proceedings, 1st International Symposium on Solid Oxide Fuel Cells," Vol. 89-11, p. 99. The Electrochemical Society, 1989.
11. De Collongue, B., Garbowski, E., and Primet, M., *J. Chem. Soc. Farad. Trans.* **87**, 2493 (1991).
12. Baker, R. T., and Metcalfe, I. S., *Appl. Cat. A: General* **126**, 297, 319 (1995).
13. Baker, R. T., Metcalfe, I. S., Middleton, P. H., and Steele, B. C. H., *Solid State Ionics* **72**, 328 (1994).
14. Kononyuk, I. F., Tolochko, S. P., and Surmach, N. G., *Inorg. Mater.* **22**, 83 (1986).
15. Tolochko, S. P., Kononyuk, I. F., Lyutsko, V. A., and Zonov, Y. G., *Inorg. Mater.* **23**, 1342 (1987).
16. Tolochko, S. P., Kononyuk, I. F., Zonov, Y. G., and Ivashkevich, L. S., *Inorg. Mater.* **23**, 743 (1987).
17. Gilbu, B., Fjellvåg, H., and Kjekshus, A., *Acta Chemica Scand.* **48**, 37 (1994).
18. Gilbu Tilset, B., Fjellvåg, H., and Kjekshus, *J. Solid State Chem.* **119**, 271 (1995).
19. Höfer, H. E., and Schmidberger, R., *J. Electrochem. Soc.* **141**, 782 (1994).
20. Höfer, H. E., and Kock, W. F., *J. Electrochem. Soc.* **140**, 2889 (1993).
21. Ganguly, P., Vasanthacharya, N. Y., Rao, C. N. R., and Edwards, P. P., *J. Solid State Chem.* **54**, 400 (1984).
22. Tai, L. W., and Lessing, P. A., *J. Mater. Res.* **7**, 511 (1992); **7**, 502 (1992).
23. Stern, E., private communication.
24. Larson, A. C., and Von Dreele, R. B., GSAS User Guide, Los Alamos National Laboratory, Los Alamos, New Mexico, 1990.
25. van Attekum, P. M. T. M., and Trooster, J. M., *J. Electron Spectrosc.* **11**, 363 (1970).
26. Tougaard, S., *Surf. Sci.* **216**, 343 (1989).
27. Scofield, J. H., *J. Electron Spectrosc.* **8**, 129 (1976).
28. Seah, M. P., and Dench, W. A., *Surf. Interface Anal.* **1**, 2 (1979).
29. Reilman, R. F., Msezane, A., and Manson, S. T., *J. Electron Spectrosc.* **8**, 389 (1976).
30. Khattak, C. P., and Cox, D. E., *Mater. Res. Bull.* **12**, 463 (1977).
31. Goodenough, J. B., Mott, N. F., Pouchard, M., Demazeau, G., and Hagenmuller, P., *Mater. Res. Bull.* **8**, 647 (1973); García-Muñoz, J. L., Rodríguez-Caravajal, J., Lacorre, P., and Torrance, J. B., *Phys. Rev. B* **46**, 4414 (1992).
32. Vidyasagar, K., Reller, A., Gopalakrishnan, J., and Rao, C. N. R., *J. Chem. Soc. Chem. Commun.* 7 (1985).
33. Rakshit, S., and Gopalakrishnan, P. S., *J. Solid State Chem.* **110**, 28, (1994).
34. Moudallal, H., Stojanovic, M., Jacobson, A. J., and Mims, C. A., to be published.
35. Frydman, A., Castner, D. G., Schmal, M., and Campbell, C. T., *J. Catal.* **152**, 133 (1995); **157**, 133 (1995).
36. Olive, G., *Surf. Sci.* **297**, 83 (1993).
37. Berthou, H., Jorgensen, C. K., and Bonnelle, C., *Chem. Phys. Lett.* **38**, 199 (1976).
38. Howng, W.-Y., and Thorn, R. J., *J. Phys. Chem. Solids* **41**, 75 (1980).
39. Lam, D. J., Veal, B. W., and Ellis, D. E., *Phys. Rev. B* **22**, 5730 (1980).
40. Esteva, J.-M., Karnatak, R. C., Fuggle, J. C., and Sawatzky, G. A., *Phys. Rev. Lett.* **50**, 910 (1983).
41. Sarma, D. D., Kamath, P. V., and Rao, C. N. R., *Chem. Phys.* **73**, 71 (1983).
42. Schneider, W.-D., Delley, B., Wuilloud, E., Imer, J.-M., and Baer, Y., *Phys. Rev. B* **32**, 6819 (1985).
43. Kotani, A., *J. Phys.* **48**, 869 (1987).
44. Imada, S., and Jo, T., *Physica Scripta* **41**, 115 (1990).
45. Torrance, J. B., Lacorre, P., Nazzal, A. I., Ansaldo, E. J., Niedermayer, Ch., *Phys. Rev. B* **45**, 8209 (1992); Sarma, D. D., Santra, A. K., and Rao, C. N. R., *J. Solid State Chem.* **110**, 393 (1994).
46. Choisnet, J., Abadzhieva, N., Stefanov, P., Klissurski, D., Bassat, J. M., Rives, V., and Minchev, L., *J. Chem. Soc. Farad. Trans.* **90**, 1987 (1994).
47. Gunasekaran, A. N., Ragadurai, S., Carberry, J. J., Bakshi, N., Alcock, C. B., *Solid State Ionics* **73**, 289 (1994).
48. Tejuca, L. G., and Fierro, J. L. G., *Thermochemica Acta* **147**, 361 (1989).
49. Tejuca, L. G., and Fierro, J. L. G., *Appl. Surf. Sci.* **27**, 453 (1987).
50. Stojanovic, M., Moudallal, H., Jacobson, A. J., and Mims, C. A., *J. Catal.* **166**, 324 (1997).
51. Derighetti, B., Drumheller, J. E., Laves, F., Müller, K. A., and Waldner, F., *Acta Crystallogr.* **18**, 557 (1965).